Evaluation of Composite Materials at Cryogenic Temperatures

Locke D. Spencer[*,1], Adam Christiansen[1], Ian T. Veenendaal[1], Sudhakar Gunuganti[2], David A. Naylor[1], Brad G. Gom[1,2], Geoffrey R. H. Sitwell[1], Navid Zobeiry[3], and Anoush Poursartip[3]

[1]Department of Physics and Astronomy, University of Lethbridge, Alberta, Canada, T1K 3M4;
[2]Blue Sky Spectroscopy Inc., Lethbridge, Alberta, Canada, T1J 0N9;
[3]Composites Research Network, University of British Columbia, Vancouver, British Columbia, Canada, V6T 1Z4.
[*]Corresponding author (Locke.Spencer@uLeth.ca)

ABSTRACT

With high stiffness, tensile strength, strength-to-mass ratio, and extremely low thermal conductivity, carbon-fibre reinforced polymers (CFRPs) are an important material for aerospace applications. This includes space-borne Far-Infrared (FIR) astronomical instrumentation which often requires operation at cryogenic temperatures. Little is known about CFRPs, however, at cryogenic temperatures. We have developed a test facility for exploring CFRP properties down to 4 K. We present results from our ongoing study in which we establish dedicated cryogenic CFRP testbed infrastructure and compare and contrast the performance of CFRP samples using different materials, and multiple layup configurations. The goal of this research is to explore the possibility of making CFRP-based, monolithic, lightweight, cryogenic astronomical instrumentation.

KEYWORDS: cryogenic, experimental astrophysics, laser metrology, coefficient of thermal expansion

1 INTRODUCTION

Far-Infrared (FIR) astrophysical observations often require space-borne instrumentation operating at cryogenic temperatures, placing stringent constraints on the launch mass as well as the mechanical and thermal properties of their support structures at low temperatures. With high stiffness, tensile strength, strength-to-mass ratio, and extremely low thermal conductivity, carbon fibre reinforced polymers (CFRPs) are an important material for aerospace and FIR astronomical applications (Enya et al., 2011; Jones et al., 2016; Tuttle et al., 2017). Well characterized instrumentation of a high Technology Readiness Level (TRL) (Web-1, 2019) is required to minimize risks associated with remote operation from vantage points such as the sun-earth second Lagrangian point, L2, where typical mission duration exceeds several years and instrument access is not practical outside of software updates. While CFRPs show promise as a potential component of future FIR space instrumentation (e.g., telescope support structures, lightweight moving components, lightweight mirrors with complex integrated backing structures), little is known about the properties of CFRP materials at cryogenic temperatures (Bechel and Kim, 2004; Grogan et al., 2014; He et al., 2013; Kanagaraj & Pattanayak, 2003; Schutz, 1998).

To this end, we are actively developing a test facility for exploring the thermal, mechanical, and optical properties of CFRPs at cryogenic temperatures (Veenendaal, 2016). This test facility operates with closed-cycle liquid-cryogen-free pulse-tube coolers (PTCs), and is thus more efficient, cost-effective, and less hazardous than wet-cryogen counterparts. The development of a cryostat for cryogenic material property investigation includes the evaluation and integration of interferometric laser metrology systems capable of operation within the cryostat and recording differential displacement at cryogenic temperatures, i.e., $\sim$4 K

(I. Veenendaal et al., 2016). This work presents the development and use of a frequency-modulated laser metrology system (Christiansen et al., 2019) coupled with a standard 1550 nm wavelength telecommunications laser (Web-2, 2019), in measuring and evaluating cryogenic properties of CFRP materials, with Aluminum samples used as a calibration reference material. Fig. 1 shows a block diagram of the frequency-modulated laser metrology system as well as a rendering of the Test Facility Cryostat (TFC) both used in this work.

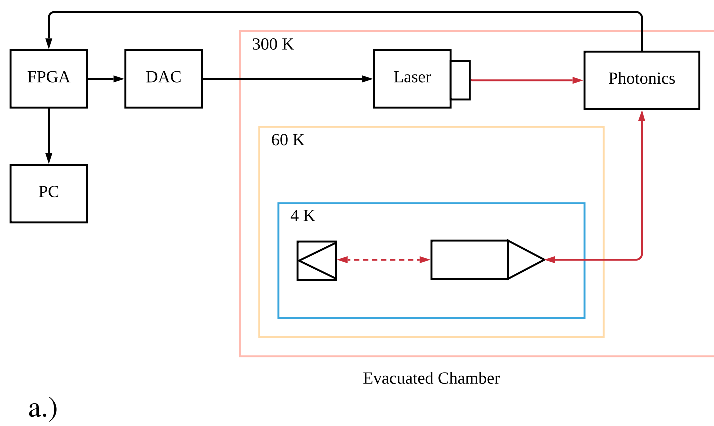

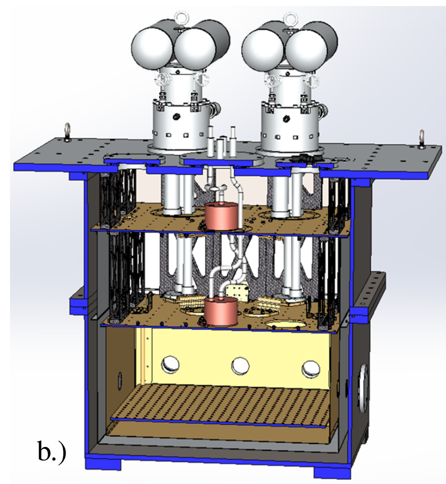

Figure 1. Cryogenic test facility. a.) Block diagram of the frequency-modulated laser metrology system including the Field-Programmable-Gate Array (FPGA) control board, Digital-to-Analog (DAC) laser controller, and a simple schematic of the laser fibre coupled with a collimator and retro-reflector in the 4 K test chamber. b.) CAD rendering of the TFC including the ∼70 liter volume 4 K test chamber in the lower portion of the image.

2 LASER METROLOGY

We have previously reported measurements of the Coefficient of Thermal Expansion (CTE) for CFRP materials at cryogenic temperatures using a laser interferometer system external to the cryostat I. Veenendaal et al. (2016); Veenendaal (2016). This modality required a window on the cryostat to allow the laser to probe the cold chamber, but this comes at the cost of increased radiant loading on the chamber, which ultimately limits the achievable base temperature. Moreover, maintaining the optical alignment of such a system through the cryostat window during thermal cycling is challenging.

Subsequent efforts focused on laser metrology capable of operation internal to the cryostat and saw the development of 3-phase (Naylor et al., 2018) and differential 3-phase laser metrology systems (Spencer et al., 2018). For cryogenic operation, the laser and photonics components operate at room temperature within the evacuated cryostat with a fibre-optic cable connecting the system to the cryogenic test chamber at 4 K. While the 3-phase technique was shown to be suboptimal for the low rates of change of displacement experienced during CTE measurements, they were essential in validating the internal laser interferometric technique including the design of the 4 K interface between the optical fibre and the free-space delay optics. A frequency-modulated laser metrology system was then developed as it reduced the number of photodiodes required by a factor of three compared to the 3-phase systems.

As shown in Fig. 1.a, the laser and photonics portion of the metrology system used in this work operate at room temperature within the evacuated cryostat and are connected to the 4 K cryogenic test chamber by a fibre-optic cable. The laser modulation scheme provides a data output rate of 1 kHz, with the current configuration requiring significant post-processing to convert the raw detector signal into quadrature phase and subsequent optical position values. The long duration of the thermal cycles in this work required sub-sampling the raw output by a factor of 200 resulting in a 5 Hz data rate on the measurement of relative

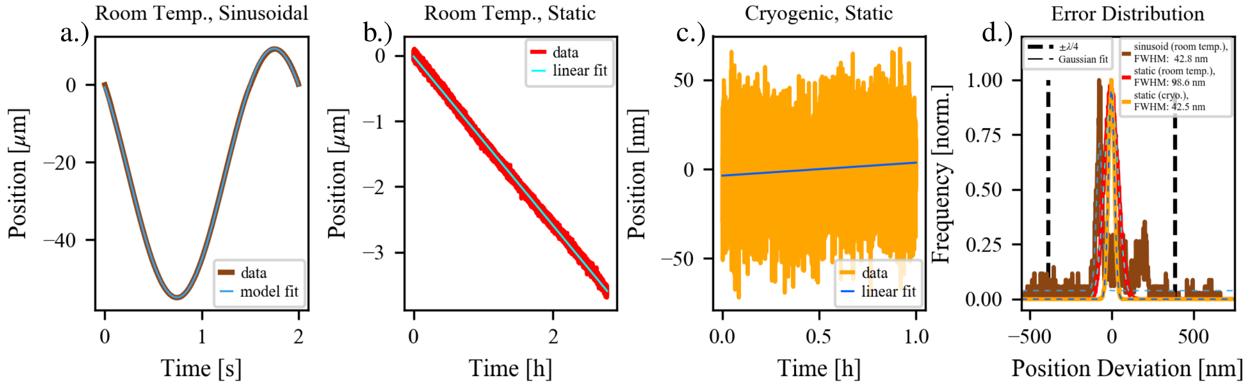

Figure 2. Validation of the frequency modulated laser metrology system: a) measurement of the sinusoidal oscillation of a piezo translation stage, b) room-temperature bench-top measurement of stationary target with a slow linear contraction as a room was cooling, c) measurement of a cryogenic stationary target, and d) histograms of the residuals for each of the previous cases. The histogram Full-Width at Half-Maximum (FWHM) is reported, where the system is most stable in an evacuated cryogenic environment demonstrating a FWHM in positional uncertainty of 43 nm.

position. The 1 kHz data rate places an upper limit of ~387 μm/s (i.e., $(\lambda/4)/\Delta t_{\text{sample}}$) on the motion under study, while the 5 Hz data rate reduces this limit to ~1.9 μm/s. A detailed explanation of the cryogenic frequency-modulated laser metrology system, based on the work of Kissinger (2015), is found in Christiansen et al. (2019).

Fig. 2 presents results from validation testing conducted on the laser metrology system. A piezo-driven linear translation stage was set to a 50 μm amplitude 50 Hz sinusoidal oscillation on a laboratory bench-top in standard atmosphere, with the metrology system recording the position over a 2 s interval at a 1 kHz sample rate. Another test case (Fig. 2.b) sampled the position of a static target at a rate of 5 Hz for several hours in an unoccupied laboratory set to slowly cool a few degrees. An additional static test (Fig. 2.c) was taken under vacuum at 4 K, sampled at a rate of 5 Hz for an hour. Histograms of the distribution of position error for each of these cases is presented in Fig. 2.d.

Although the FWHM of the position error observed for the first test case was 43 nm, the error distribution has a non-zero floor and deviates from a normal distribution curve. For this trial, with position sampled at a rate of 1 kHz for 2 s, these deviations are attributed to a dynamic free-space optical path in the laboratory. The error distribution for the second case has a FWHM of 99 nm with a Gaussian shaped distribution. Without laboratory atmosphere in the optical path, and with a stable temperature, the cryogenic position follows a normal distribution with a FWHM of 43 nm. With the effect of laboratory atmospheric changes removed from the system, the laser metrology system is shown to have a precision of <50 nm.

3 THERMAL CYCLING AND CRYOGENIC TESTING

Table 1. Fibre orientations for CFRP sample types.

Configuration	Layer orientation (fibre axis angle with respect to length axis)
Parallel	0° / 0° / 90° / 0° / 0° / 90° / 0° / 0°
Orthogonal	90° / 90° / 0° / 90° / 90° / 0° / 90° / 90°

Fig. 3 presents the 4 K portion of the test setup. At the cold terminus of the fibre, a collimator launches a parallel beam to a corner cube retro-reflecting prism which returns the beam to the collimator, and ultimately the fibre, in order to measure the linear expansion of the sample material under thermal cycling between 4 K and room temperature. Also visible in the figure are temperature sensors on various portions of the test harness, mounted to the sample plates using GE-varnish (Cude & Finegold, 1971). Table 1 provides the fibre-orientation used in fabricating the CFRP samples. Thermal cycle tests of both the parallel and orthogonal configurations were conducted, although position measurements are only presented for the parallel configuration (see §4). Fig. 4 presents the observed temperatures and relative position measurements for the experiments presented in this work. Note that the CFRP thermal cycle time is longer than that of Aluminum.

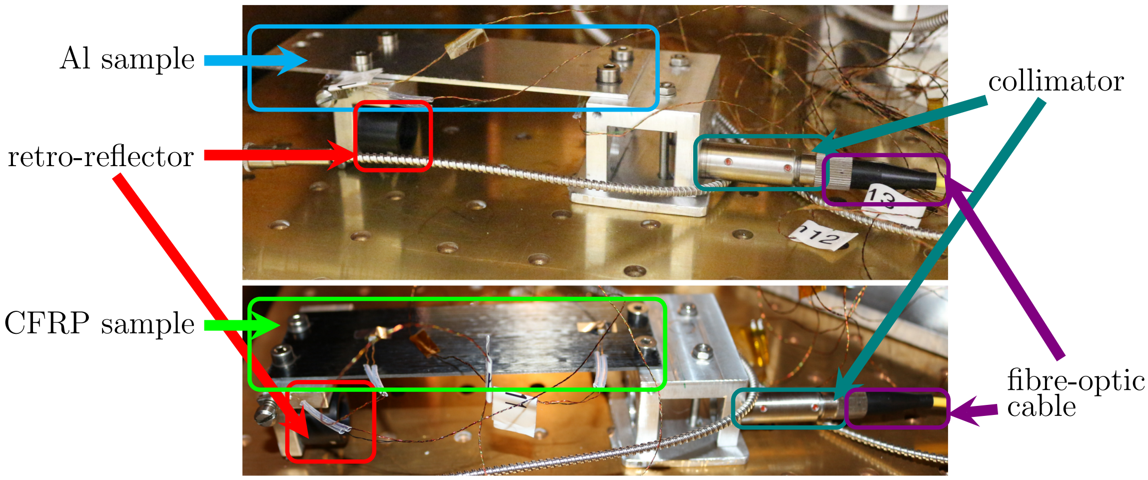

Figure 3. Samples under test in the 4 K test chamber, including Aluminum (top) and CFRP (bottom), and the cryogenic portion of the laser metrology system.

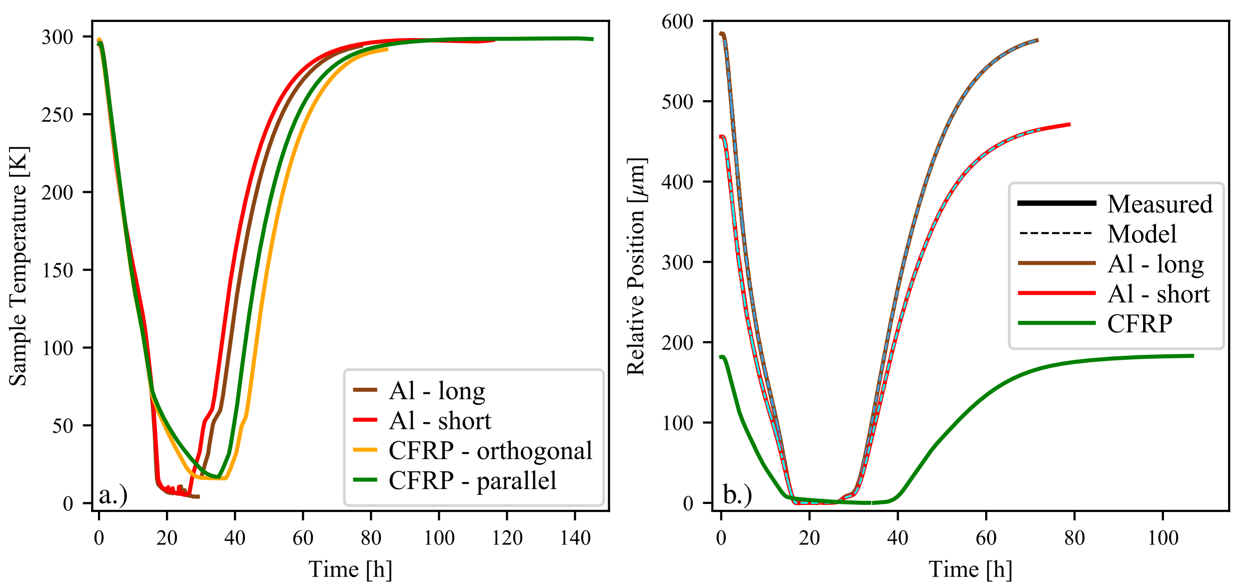

Figure 4. Recorded time series data of the sample temperature (a.) and position (b.) measurements.

4 RESULTS AND ANALYSIS

Test results were analyzed in order to determine the relative thermal expansion/contraction of the CFRP sample. Raw data were moderately smoother and interpolated onto common abscissa vectors to allow comparison and data processing. Calibration measurements were conducted using two different lengths of the Aluminum sample, with the results for the cool-down and warm-up portions of the observation treated separately. This differential measurement of the Aluminum sample allows for the removal of any length contraction effects caused by other portions of the test harness along the optical axis. The cool-down portion of the thermal cycle requires the closed-cycle PTC compressor to be engaged and thus the vibrational environment inside the cryostat is higher than the warm-up phase with the compressor turned off. Fig. 5.a illustrates the subtraction of the long and short Aluminum sample data, and compares these results with the accepted value (J. Ekin, 2006; Web-3, 2019) for a 27.54 mm sample length difference for Aluminum. This isolated Aluminum measurement can then be scaled to the sample lengths for each trial, and removed to isolate the thermal expansion associated with the test harness alone, i.e., everything else undergoing thermal expansion/contraction apart from the sample plate. Fig. 5.b illustrates the resultant isolated test harness systematic component of thermal expansion associated with each test case, some vertically offset for clarity. Although there are differences in the isolated systematics between the cool-down and warm-up regions, there is very good agreement between different cool-down or warm-up cycles for both cases. The feature in the cool-down data at ∼200 K is under investigation. As the warm-up results are smoother, and the vibration environment is lower in the warm-up case, this will be used in the evaluation of the thermal expansion of the CFRP samples.

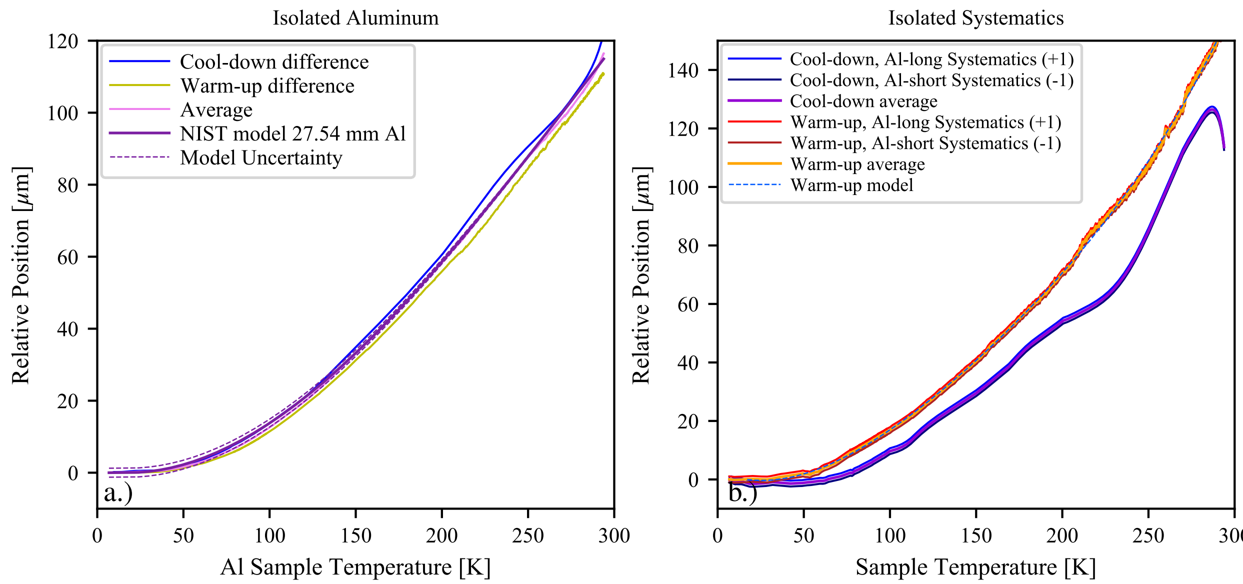

Figure 5. Intermediate data products used to verify performance and determine the linear expansion of the test samples. a) Residual from the long and short Al test samples resulting in the removal of any systematic effects from the measurement, compared against the NIST model for Al using the measured length of 27.5(4) mm. b) Using the result of (a), scaled for each trial, the systematic length contraction for both cool-down and warm-up thermal cycles. The warm-up data is used in the analysis presented for CFRP.

The measurements of the thermal contraction/expansion for the orthogonal CFRP sample are not shown as a result of an issue in the data collection for this test case. A possible explanation for the observed issue is that this sample experienced a series of micro-fractures during the cool-down portion of the thermal cycle, and although the average rate of contraction over the cooling time is expected to be well below the maximum velocity threshold of ∼1.9 μm/s, the instantaneous velocity during a micro-fracture event could exceed this limit and result in errors in the reported position values. Preliminary investigation indicates that the sample rate of 5 Hz is insufficient for the rate of length change along the CFRP axis perpendicular to the fibre direction. The metrology system is capable of recording at much faster data rates, but not for the duration (e.g., >48 h) of this test. A change in hardware configuration and FPGA control software currently under development will overcome this obstacle and should allow monitoring of micro-fractures during thermal cycling in real time.

Fig. 6.a presents the observed change in relative position as a function of sample temperature for the two Aluminum test cases and the parallel fibre-orientation CFRP sample. The figure also shows the CFRP

result with the linear expansion of the test-harness removed. Fig. 6.b presents the relative expansion ($\Delta L/L$) in units of parts-per-million (PPM) for the isolated CFRP data, along with a 4$^{\text{th}}$ order polynomial fit to this data.*

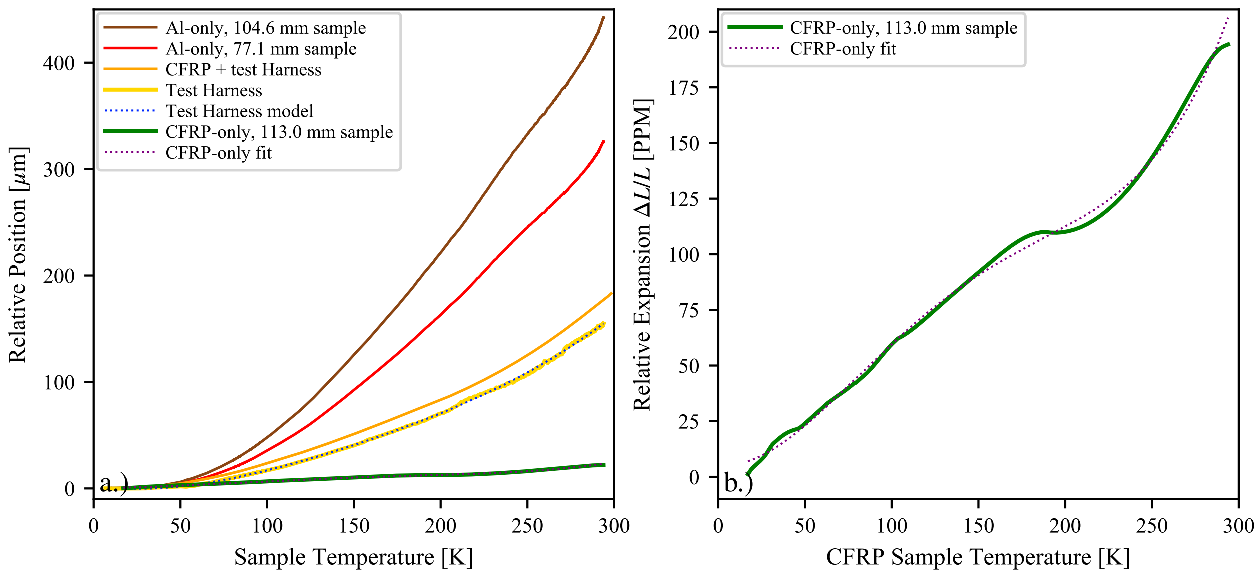

Figure 6. Test sample measurements during thermal cycle experiments: a.) both Aluminum trials with the systematic component removed, and the CFRP-parallel fibre orientation trial both with and without the systematic component included, as well as the differentially determined test harness profile for comparison; b.) a length-normalized plot of the CFRP linear expansion observed during the warm-up portion of the trial, with polynomial fit.

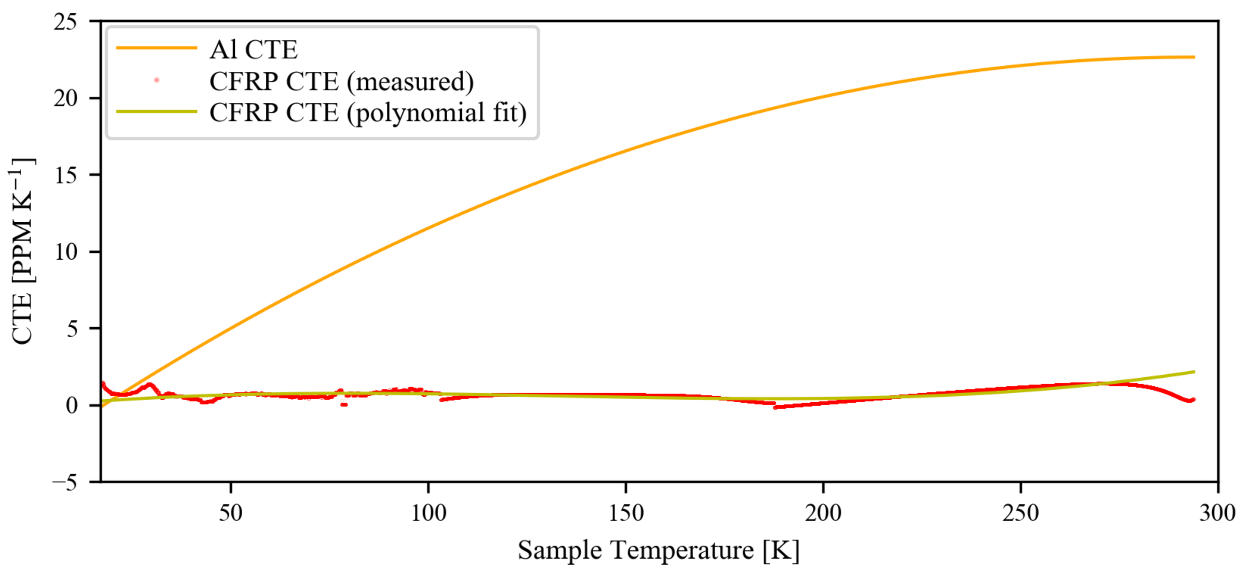

Figure 7. CTE values for both Al and CFRP samples.

The calculated CTE for both the Aluminum and CFRP samples is shown in Fig. 7, along with the results obtained from deriving the CTE values using a 4$^{\text{th}}$ order polynomial fit of the measured linear expansion data (i.e., ΔL). The data give a CFRP CTE of order 0.7 ± 0.4 [PPM K^{-1}] for the CFRP sample along the fibre axis. Some of the scatter in this data is resultant from sampling metrology data at 5 Hz at

*NIST(Web-3, 2019) provides thermal linear expansion models in such a format.

an intermediate stage, and will be resolved when this processing is implemented on-board the FPGA data acquisition system. This will also address problems identified with the metrology data for the measurement of CFRP CTE orthogonal to the fibre axis, which should be available as the next version of this system is developed.

5 CONCLUSIONS AND FUTURE WORK

We have characterized the behaviour of the test harness developed to measure the CTE of CFRP and other samples, and measured the relative thermal expansion ($\Delta L/L$) and CTE for CFRP material. Improvements underway in the frequency-modulated laser metrology system will allow for higher data rates in monitoring thermal expansion/contraction of sample materials. Initial results indicate that we may also be able to monitor micro-fracturing induced vibration in CFRP samples under cryogenic conditions in real time. Optical monitoring of sample vibration under cryogenic conditions will also allow for the evaluation of stress deformation and Young's modulus by monitoring the vibrational resonance frequency of a sample as a function of sample temperature. Ongoing work includes improving the precision of the CFRP thermal expansion measurements and comparing results for different sample materials and fibre lay-up orientations. The custom-developed fibre-fed laser metrology system, capable of operation under vacuum inside a cryostat and with differential displacement metrology at 4 K sample temperatures, has shown nm-level residuals for both moving and stationary targets over time periods of hours.

ACKNOWLEDGMENTS

The authors thank Rebecca Sirota for her assistance in the design and fabrication of the differential metrology electronics. This work acknowledges the support of the Canadian Space Agency (CSA), Canadian Foundation for Innovation (CFI), Alberta Research Capacity Program (RCP), the Natural Science and Engineering Research Council of Canada (NSERC), the Canada Microelectronics Corporation (CMC), and the Canada Research Chair (CRC) programs.

References

Bechel and Kim. 2004, Composites Science and Technology, 64, 17731784. Damage trends in cryogenically cycled carbon/polymer composites

Christiansen, Naylor, Veenendaal, & Gom. 2019, A frequency-modulated laser interferometer for nanometer-scale position sensing at cryogenic temperatures

Cude, J. & Finegold, L. 1971, Cryogenics, 11, 394 . Specific heat of GE 7031 varnish (4–18 K)

Enya et al. 2011, Cryogenics, 52, 86. High-precision CTE measurement of hybrid C/SiC composite for cryogenic space telescopes

Grogan et al. 2014, Composites: Part A, 66, 237. Damage characterisation of cryogenically cycled carbon fibre/PEEK laminates

He et al. 2013, Composites: Part B, 44, 533. Micro-crack behavior of carbon fiber reinforced thermoplastic modified epoxy composites for cryogenic applications

I. Veenendaal et al. 2016, in Proc. SPIE, Vol. 9904, 99045E

J. Ekin. 2006, Experimental Techniques for Low-Temperature Measurements: Cryostat Design, Material Properties and Superconductor Critical-Current Testing (UK: Oxford University Press)

Jones et al. 2016, in Proc. SPIE, Vol. 9904, 99046F

Kanagaraj, S. & Pattanayak, S. 2003, Cryogenics, 43, 399. Measurement of the thermal expansion of metal and FRPs

Kissinger, T. 2015, PhD thesis, Cranfield University (UK)

Naylor, D., Veenendaal, I., Gom, B., & Christiansen, A. 2018, in Society of Photo-Optical Instrumentation Engineers (SPIE) Conference Series, Vol. 10539, Photonic Instrumentation Engineering V, 105390T

Schutz, J. 1998, Cryogenics, 38, 3. Properties of composite materials for cryogenic applications

Spencer, L. D., Veenendaal, I. T., Naylor, D. A., et al. 2018, in Society of Photo-Optical Instrumentation Engineers (SPIE) Conference Series, Vol. 10706, Advances in Optical and Mechanical Technologies for Telescopes and Instrumentation III, 107063R

Tuttle et al. 2017, Cryogenics, 88, 36. Cryogenic thermal conductivity measurements on candidate materials for space missions

Veenendaal, I. T. 2016, Master's thesis, University of Lethbridge (Canada)

Web References:

Web-1. 2019, The ESA Science Technology Development Route, http://sci.esa.int/sci-ft/50124-technology-readiness-level/

Web-2. 2019, Eblana Photonics Corporation, www.eblanaphotonics.com

Web-3. 2019, National Isntitute of Standards and Technology, https://trc.nist.gov/cryogenics/materials/6061%20Aluminum/6061_T6Aluminum_rev.htm